Title: **Identification of intrinsic group differences in predictive anticipatory biasing of pain during uncertainty: preparing for the worst but hoping for the best**

Authors: Irina A. Strigo, Molly Kadlec, Jennifer M. Mitchell, and Alan N. Simmons.

Methods:

Supplementary Material 1: Detailed Explanation of Pain-Anticipation Paradigm

Each fMRI session included two acquisitions (i.e., Run 1 and Run 2) of the pain-anticipation paradigm, separated by 5-7 mins. The stimulation was delivered through a 9cm^2 thermode (Medoc TSA-II, Ramat-Yishai, Israel) on the participant's left forearm, as described elsewhere [7]. The schedule of stimuli differed between imaging runs in a pseudorandom and counterbalanced order. The periods of anticipation were ten seconds long and began with a cue that signaled high, low, or uncertain level of pain. More specifically, ten seconds prior to the onset of pain, the participants were presented with an image of a colored cross. A red cross indicated a temperature stimulus producing moderate levels of heat pain or "high-pain, HP", a green cross indicated a temperature stimulus producing low levels of heat pain or "low-pain, LP", and a yellow cross, indicated pain of uncertain intensity (at 50% probability being high or low, which was not known to the subject). These anticipation periods were followed by seven seconds of either high or low-pain. The high-pain stimulation was administered at 47.5ºC and the low-pain stimulation at 45.5ºC, both of which had a rise and fall rate of 10ºC/sec. Note that both levels of temperature simulations were painful to the subject and they were not informed that only two levels of temperature stimulation would be delivered. In all instances when the level of pain was cued, the participant received the corresponding level of pain. When an uncertain cue was given, the participant was administered either the HP or LP stimulation. Each temperature stimulus was followed by a period of rest, signaled by a change in the color of the cross to blue, that was jittered between 24 to 30 seconds (aside from the short period of rest before the first anticipation cue in each session, which lasted 7 and 10 seconds, respectively). Each session included 14 separate anticipation-pain conditions and lasted a total 618 seconds. In Run 1, there were three HP-cued conditions and four LP-cued conditions. The other seven conditions began with an uncertain cue (UN), three of which were followed by low-pain delivery, and four with high-pain. In Run 2, there were four HP conditions, three LP conditions, and of the seven UN conditions, four were followed with low-pain and three were followed with high-pain. In combination, there was a total of seven HP, seven LP, and fourteen UN (with seven LP and seven HP) conditions (**Supplementary Figure SM1**).

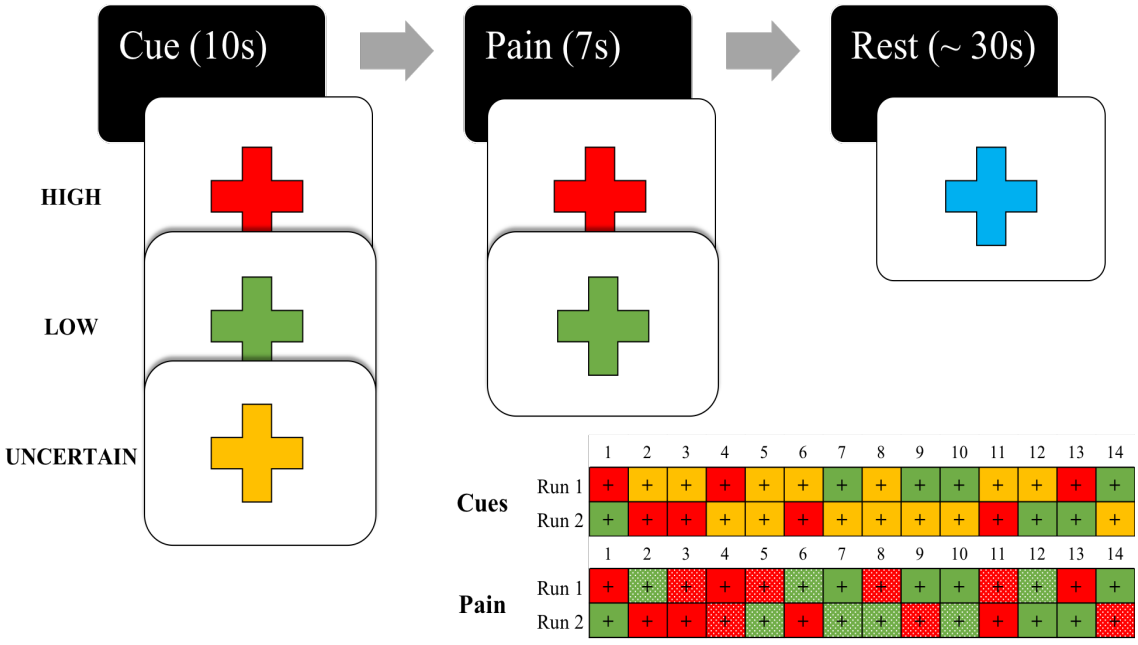

Supplementary Figure SM 1: Schedule of pain-anticipation paradigm. Simple breakdown of ordered pain-anticipation-rest timeline. Cues appear as presented to subjects. RED represents high-pain cue followed by high-pain administration (HP). GREEN represents low-pain cue followed by low-pain administration (LP). YELLOW represents uncertain pain cue followed by either high or low-pain administration (UN). Bottom right: timeline for one complete imaging session (both run 1 and run 2) separated by anticipation cue timeline (HP, LP, and UN), and pain stimulation (HP and LP).

Supplementary Material 2: CONN Preprocessing Pipeline.

Preprocessing was completed using the default preprocessing pipeline in CONN. The pipeline included the following consecutive steps: (1) functional realignment and unwarp, (2) functional center to (0,0,0) coordinates, (3) functional slice-timing correction, (4) functional outlier detection, (5) functional direct segmentation and normalization, and (6) functional smoothing. For the functional outlier detection (step 4) the intermediate settings were chosen with 97th percentile in the normative sample. For segmentation and normalization (step 5), default tissue probability maps were used for the simultaneous segmentation of gray, white and cerebrospinal fluid (CSF) and Montreal Neurological Institute (MNI) coordinate normalization. The smoothing kernel used in the functional smoothing (step 6) was 4mm full-width half-maximum (FWHM). Next, denoising was performed on the functional data. For denoising, linear detrending and regression of the confounding effects of realignment and scrubbing was completed. Despiking was implemented before regression and a band pass filter of [0.008Hz, infinity] was applied after regression.

Supplementary Material 3: Region of Interest (ROIs) mask

Masks of selected ROIs were created in MNI space using AFNI and Hammers atlas[3; 5]. A total of twenty-six ROIs were chosen based on their prominent roles in pain prediction, processing and relief[1; 2; 4] (see **Supplementary Figure SM3**).

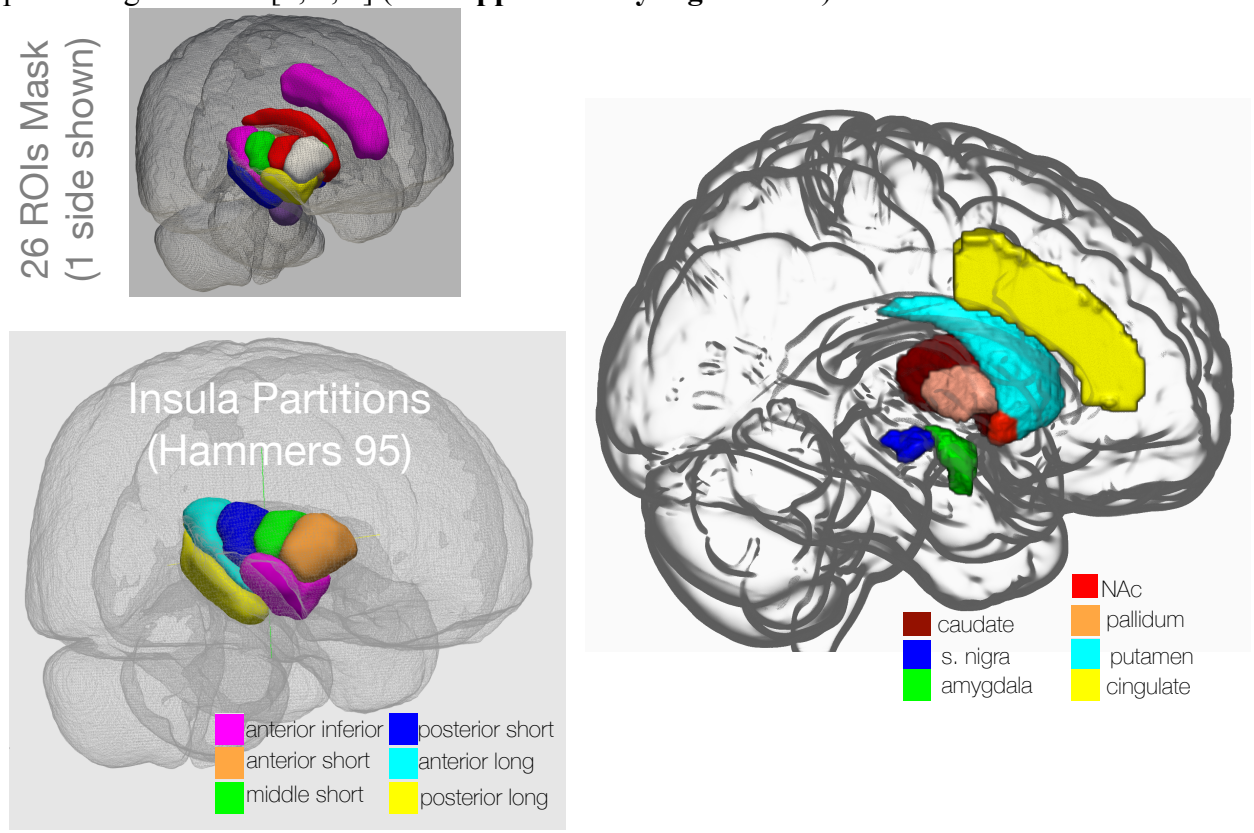

Supplementary Figure SM3: ROI masks used in the MVPA analyses (Hammers 95)

Supplementary Material 4: Optimal model parameters.

Optimal parameters for the elastic net model were: alpha optimized based on single-subject accuracy, lambda optimized based on the minimum cross-validated lambda per subject over one hundred validation runs, and misclassification error ("class") used as the loss parameter. In accordance with previous findings [6], the t-statistic was found to be superior to the beta-coefficient-based activation maps. Model performance and alpha optimization are depicted in **Supplementary Figure SM4**.

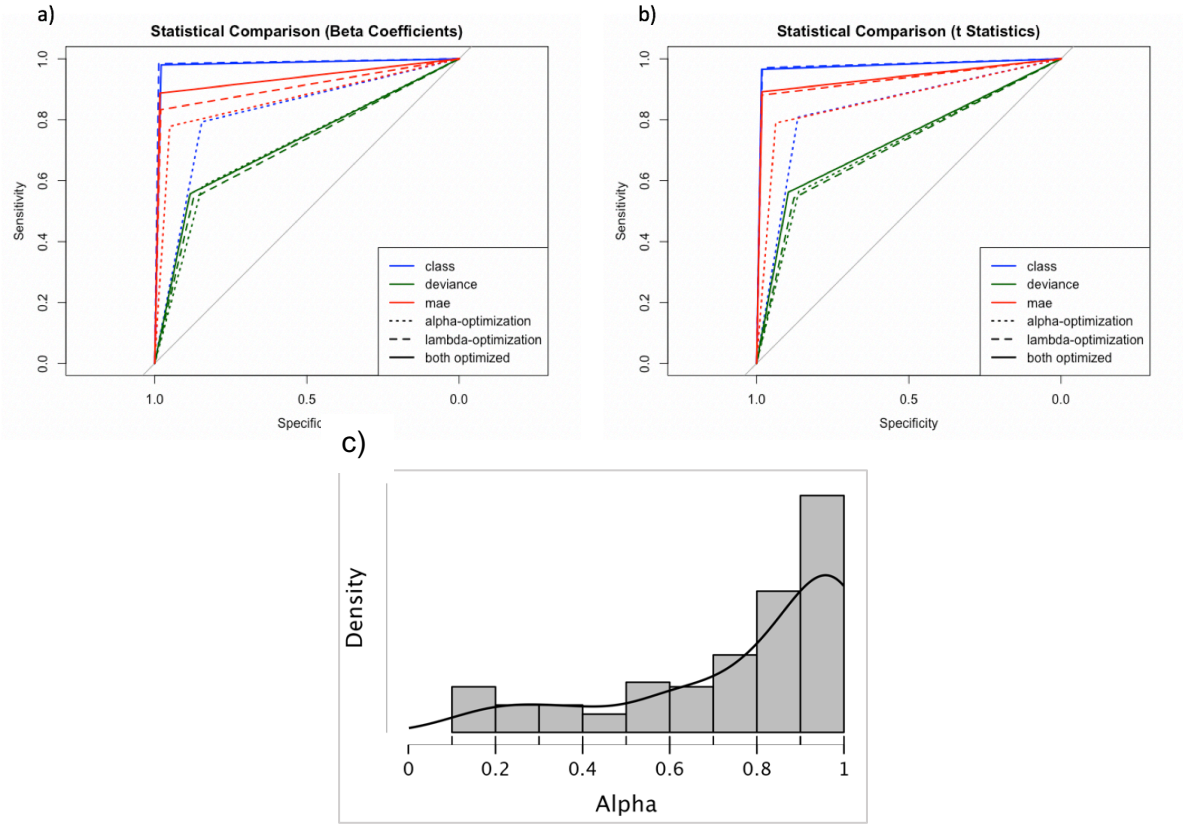

Supplementary Figure SM4: Receiver Operating Characteristic (ROC) curves for elastic model setup results. (a) beta-coefficient activation maps and (b) t-statistic activation maps. Loss parameter used in the cross-validation step was varied between trials such that; "class": misclassification error; "deviance": squared error; "mae": mean absolute error. (c) Distribution of the optimized alpha in the entire sample

Results:

Supplementary Material 5: Whole brain activation tables during pain anticipation

Brain Region	Volume (voxels)	x	y	z	z score
Low Pain Anticipation					
L. Precuneus	15664	-12	-53	26	-4.9
L. Ventromedial PFC	4394	-7	51	9	-5
R. Postcentral Gyrus	1725	44	-20	53	-5
R. Inferior Frontal Gyrus	1220	47	22	30	4.8
R. Inferior Parietal Lobule	1059	42	-52	43	4.6
R. Inferior Occipital Gyrus	937	34	-92	-4	5.1
L. Inferior Occipital Gyrus	777	-31	-95	-7	6.5
R. Superior Parietal Lobule	400	18	-54	61	-6
L. Inferior Temporal Gyrus	390	-57	-7	-27	-4.5
R. Fusiform Gyrus	374	28	-40	-19	-4.6
L. Inferior Parietal Lobule	318	-42	-53	45	4.9
L. Middle Temporal Gyrus	278	-54	-21	0	-4.6
R. Middle Frontal Gyrus	250	36	52	0	4.5
R. INSULA (RAI)	223	37	25	-6	4.5
R. Superior Temporal Gyrus	214	45	-16	-11	-4.6
T. Middle Temporal Gyrus	139	51	2	-30	-4.5
R. SMA/cingulate	128	5	27	46	4.5
R. Parahippicampal Gyrus	114	22	-17	-35	-4.4
L. Fusiform Gyrus	108	-19	-4	-39	-4.4
L. Middle Frontal Gyrus	107	-37	47	1	4.4
R. Middle Frontal Gyrus	101	25	34	41	-4.4
High Pain Anticipation					
L. Precuneus	49354	-2	-30	25	-4.6
R. INSULA (RAI)	4539	41	26	9	6
R. SMA/cingulate	2028	7	18	54	5.7
R. Middle Frontal Gyrus	1466	23	29	44	-5.5
R. Inferior Parietal Lobule	1310	55	-46	40	5.9
L. INSULA (LAI)	1289	-37	22	-5	5.7
L. Cerebellum	704	-39	-70	-36	6
L. Middle Occipital Gyrus	564	-29	-97	-8	4.7
R. Inferior Occipital Gyrus	557	33	-94	-5	5.6
L. Inferior Parietal Lobule	513	-57	-48	43	5.9
L. Middle Frontal Gyrus	477	-38	50	17	4.9
R. Posterior Cingjulate Cortex	277	0	-20	28	4.8
HP vs LP Anticipation					
R. INSULA (RAI)	626	39	26	-8	4.8
R. Precentral Gyrus	529	44	-19	57	-4.7
R. Paracentral Lobule	404	2	-26	66	-4.7
R. SMA	337	11	10	67	4.6
R. Inferior Parietal Lobule	255	64	-39	33	4.6
L. INSULA (LAI)	216	-38	23	-7	4.5
L. Inferior Parietal Lobule	165	-59	-42	38	4.5
R. Middle Temporal Gyrus	146	50	-67	0	-4.4
L. Postcentral Gyrus	121	-48	-22	53	-4.4
R. Angular Gyrus	104	49	-67	30	-4.4

Supplementary Material 6: Most Deterministic Regions

The adaptable single-subject elastic net model was designed to select the regional neural activities within 26 ROIs most significant to distinguish between certain anticipations of high and low-pain intensity. On average, 8.1 ± 2.8 regions were selected as variables with predictive value in single-subject Elastic Net models. Frequency map of regions of interest included in single-subject models are depicted in **Figure 2b**. The most frequently included regional neural activity predictor of low versus high-pain anticipation were Nucleus Accumbens and anterior short insular gyrus on the right hemisphere. Activation within these regions were included in 94 (64%) and 93 (63%) subjects' elastic net models, respectively. At a significance level of 0.05 with 26 regions, significance was determined at $p<0.0019$. There was no significant difference in incidence of regional determinism between healthy controls as compared to the "mixed psychiatric" group. Within replication sample the same regions were highly deterministic.

Supplementary Material 7: Elastic Net Model Stability

The models were consistent in the selection of relevant predictors across two runs (in Session1), between healthy and mixed psychiatric cohorts and between two experimental sessions conducted ~1 year apart. Of the thirty-two replication subjects, 29 (90.6%) of the subjects' models included the same predictors as the model created in the full cohort processing (see **Supplementary Figure SM7**). Since replication cohort included individuals (n=24) who met criteria for major depressive disorder (MDD) at the initial fMRI session, we explored whether MDD diagnosis or current depressive symptom severity influenced uncertain anticipatory biases in these subjects. Seven of the subjects were considered remitted by their second imaging session. We found that among the MDD subjects anticipatory biases were not influenced by their current diagnosis (t=0.13, p=0.90, df=31 or depressive symptom severity (t=0.98, p=0.33, df=31). These results point that affective biasing during uncertainty as determined by neural activity patterns are likely represent a stable trait characteristic of an individual.

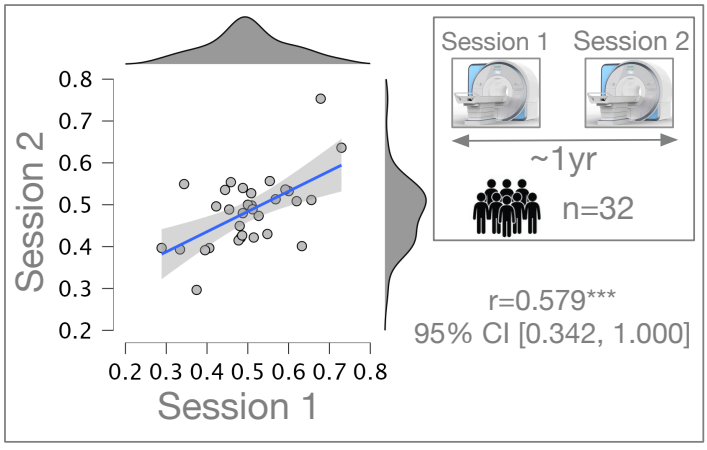

Replication Cohort	**8 Healthy Controls**	**24 MDD**		
	Mean	*Mean*	*t / χ²*	*p*
Demographic Variables				
Gender	8M/0F	17M/7F	1.16	0.28
Age (years)	27.1 ± 4.14	26.9 ± 7.2	-0.07	0.94
Race			1.08	0.78
African American	*N*=4	*N*=13		
Asian	*N*=2	*N*=9		
Caucasian	*N*=1	*N*=2		
Other	*N*=1	*N*=0		
BDI2 Progression				
BDI2 at Session 1	4.63 ± 4.9	24.7 ±	-6.3	**<0.001**
BDI2 at Session 2	4.5 ± 4.1	8.25	-2.6	**0.014**
Remitted		15.25 ± 11		
		N=7		

MDD – Major Depressive Disorder (DSM IV); BDI2 – Beck Depression Inventory

Supplementary Figure SM7: Scatter plots showing strong positive correlation between anticipatory bias predictions between Session 1 and Session 2 conducted ~1 year apart in 32 subjects from the original cohort.

Supplementary Material 8: Cluster classification stability. In order to support that clusters as defined by MixAK model were reproducible, we repeated clustering using K-means. For K-means the average probability scores from the unknown cues were used. Three clusters were identified, consistent with our MixAK results (X-squared = 150.2, df = 4, p-value < 2.2e-16). The two models classify the outer bounds (K-means 1 and 3 below) the same, however the division of the middle or unbiased group differed such that 36.7% of the sample was in the middle/unbiased group in the mixAK model and 73.5% was classified into the middle/K=2 group in the K-means model. The reported significance in the PCS helplessness was replicated in the K-means groups (F=6.258, p=0.002).

	MixAK:2/Low	MixAK:0/Unbiased	MixAK:3/High
Kmeans:K=1	40	0	0
Kmeans:K=2	15	45	20
Kmeans:K=3	0	0	27

Supplementary Material 9: Anticipatory Response Biases during Uncertainty are Related to Cognitive Coping Styles

All subjects filled out PCS< BDI-2, TAS-20 and STAI-trait measures. We first examined whether subjects in the two well-defined and stable neural clusters (olive and pink, **Figure 3A**) could be separated on the behavioral self-reported measures related to emotional and pain regulation. The results of logistic regression (GLM r) and robust regression as shown below:

Logistic Regression (MixAK clusters)	Estimate	Std. Error	z value	Pr(>|z|)	
(Intercept)	1.20737	1.1067	1.09	0.275	
BDI2	0.01922	0.02859	0.67	0.501	
PCS_Rumination	-0.15344	0.09019	-1.7	0.089	.
PCS_Ramification	0.00398	0.13784	0.03	0.977	
PCS_Helplesseness	**0.22603**	**0.08049**	**2.81**	**0.005**	**
TAS20_DifficultyID	-0.06102	0.05516	-1.11	0.269	
TAS20_DifficultyDescr	0.14402	0.07248	1.99	0.047	*
TAS20_ExternallyOrientedThinking	-0.09189	0.05659	-1.62	0.104	
STAI_T_TOTAL	-0.02902	0.02929	-0.99	0.322	

Robust Regression (MixAK clusters)	Estimate	Std.Error	t	Pr(>|t|)	
(Intercept)	2.294575	0.347127	6.61	7.70E+10	***
BDI2	0.005322	0.008332	0.64	0.524	
PCS_Rumination	0.033761	0.024912	1.36	0.1776	
PCS_Ramification	0.000257	0.044695	0.01	0.9954	
PCS_Helplesseness	**0.056598**	**0.021212**	**2.67**	**0.0085**	**
TAS20_DifficultyID	0.030328	0.016901	1.79	0.0749	.
TAS20_DifficultyDescr	**0.046734**	**0.022558**	**2.07**	**0.0402**	*
TAS20_ExternallyOrientedThinking	0.024462	0.017844	1.37	0.1726	
STAI_T_TOTAL	0.000208	0.009741	0.02	0.983	

We repeated logistic regression on clusters identified by k-means clustering and found that PCS_helplessness further differentiated all three classes.

Logistic Regression (k-means clusters)	Estimate	Std. Error	z value	Pr(>|z|)	
(Intercept)	1.8048	0.9346	1.93	0.053	.
BDI2	0.0419	0.0241	1.74	0.083	.
PCS_Rumination	-0.0674	0.0744	-0.91	0.365	
PCS_Ramification	-0.1086	0.1221	-0.89	0.374	
PCS_Helplesseness	**0.1456**	**0.0724**	**2.01**	**0.044**	*
TAS20_DifficultyID	0.0319	0.0492	0.65	0.517	
TAS20_DifficultyDescr	0.0136	0.0597	0.23	0.82	
TAS20_ExternallyOrientedThinking	-0.0541	0.0498	-1.09	0.277	
STAI_T_TOTAL	-0.0221	0.0248	-0.89	0.372	

Supplementary Material 10: Anticipatory Response Biases during Uncertainty are Related to Brain Structure

Morphometric measures including total gray matter volume in mm^3 were estimated using ANTs built-in functions for 26 regions-of-interest (ROI). The relative ICV-to-template size was determined by calculating the determinant of the affine registration matrix from the ANTs registration. The relative intracranial volume (ICV) value was then multiplied by the ICV of the MNI-152 template to calculate a total ICV value per subject). Out of these 26 regions, only the volume of the right anterior short insular gyrus was significantly and inversely associated with the average anticipatory response bias during uncertain trials (Pearson correlation coefficient r=-0.262, $p<0.05$, corrected for multiple comparisons, df=145, **Supplementary Figure SM10**), indicating that those with the greatest right anterior short insular gyrus volume were more likely to anticipate low pain during uncertainty (i.e., more likely to show a "positive bias").

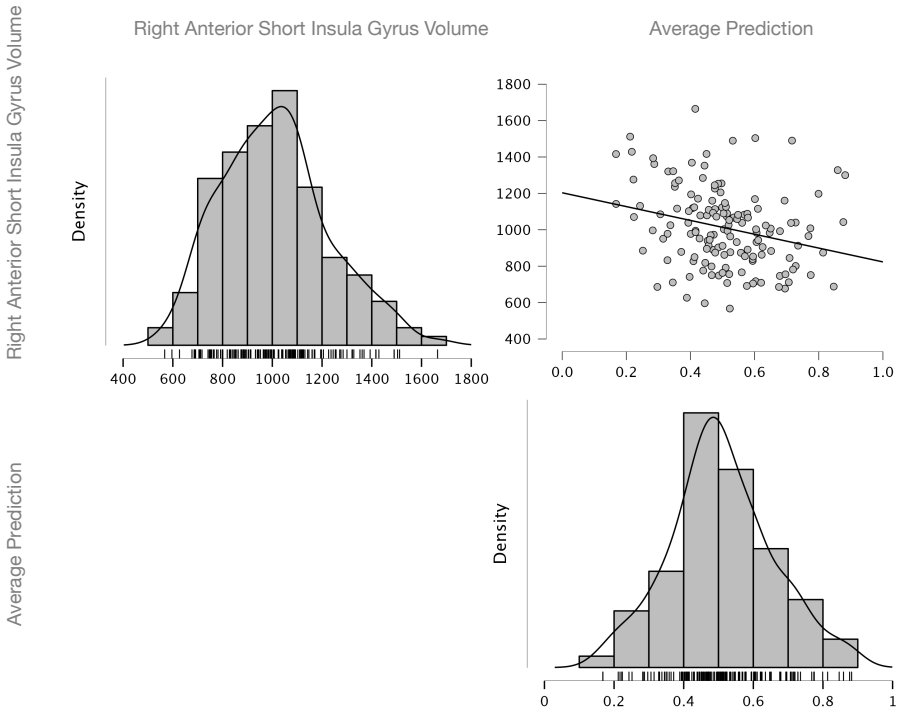

Supplementary Figure SM10: ***Scatterplot comparison of average prediction per subject versus the volume of the insular anterior short gyrus on the right hemisphere****. After correction for multiple comparisons only this region showed significant and inverse correlation (Pearson=-0.262, p=0.001) average anticipation probabilistic prediction across 14 uncertain trials plotted versus volume of insular anterior short gyrus on the right hemisphere in voxels (1 x 0.97 x 0.97 mm^3)*

Supplementary Material 11: Whole brain activation tables during pain stimulation

Brain Region	Volume (voxels)	x	y	z	Z stat
	Known Cue				
Positive Bias Group					
Left_Precuneus/PCC	25671	-10	-45	40	-3.1
Right_Insula (incl. right striatum)	11525	46	1	6	5.6
Left_Insula	3336	-42	6	-5	6.3
Right_Precentral_Gyrus	2183	45	-16	50	-5.8
Right_Cerebellum	2012	35	-38	-31	-5.9
Left_Ventromedial Prefrontal	1877	-3	51	-16	-4.9
Left_Precentral_Gyrus	1509	-61	-31	28	5.2
Right_Anterior_Cingulate_Cortex	1401	3	24	35	5.4
Right_Middle_Temporal_Gyrus	890	54	5	-31	-5
Left_Cerebellum	472	-35	-74	-38	4.8
Left_Inferior_Temporal_Gyrus	370	-39	12	-41	-4.5
Unbiased Group					
Left_Precuneus/PCC	29838	-2	-38	40	-4.1
Right_Insula	5390	46	3	4	5.4
Left_Insula	1823	-42	8	-4	5.5
Left_Ventromedial Prefrontal	1816	-1	40	-24	-5.1
Right_Middle_Temporal_Gyrus	831	55	3	-31	-5.4
Left_Inferior_Temporal_Gyrus	527	-47	3	-35	-4.8
Left_Cerebellum	389	-32	-72	-44	4.6
Right_Striatum	371	8	-7	-2	4.6
Left_Superior_Frontal_Gyrus	328	-14	65	9	-4.7
Right_Anterior_Cingulate_Cortex	307	3	24	30	4.5
Negative Bias Group					
Right_Insula (incl. right striatum)	12386	46	0	8	5.9
Left_Superior_Occipital_Gyrus	5787	-20	-63	23	-6
Left_Precentral_Gyrus	4151	-29	-21	56	-4.8
Left_Insula	3277	-42	5	-5	5
Right_Middle_Occipital_Gyrus	2210	41	-75	25	-5.4
Right_Precentral_Gyrus	1660	48	-14	47	-5.1
Right_Anterior_Cingulate_Cortex	1624	4	11	27	5.7
Left_SupraMarginal_Gyrus	1375	-61	-28	25	4.8
Left_Ventromedial Prefrontal	779	-2	42	-23	-5.1
Right_Fusiform_Gyrus	750	39	-38	-27	-4.7
Left_Middle_Frontal_Gyrus	693	-25	30	44	-4.6
Left_Superior_Medial_Gyrus	362	-12	67	11	-4.7
	Unknown Cue				
Positive Bias Group					
Left_Precuneus/PCC	22717	-7	-33	45	-6
Right_Insula	8783	48	-1	11	5.5
Left_Insula	1828	-40	14	-4	5.6
Left_Ventromedial Prefrontal	1632	-2	58	-8	-5.1
Right_Middle_Occipital_Gyrus	1626	41	-74	29	-4.8
Right_Cerebellum	965	33	-35	-30	-5.2
Left_Inferior_Parietal_Lobe	937	-60	-39	36	4.8
Right_Anterior_Cingulate_Cortex	639	4	29	42	5.2
Right_Striatum	533	9	1	-4	4.8
Right_Posterior_Cingulate_Cortex	470	3	-22	28	4.7
Right_Inferior_Temporal_Gyrus	428	48	7	-35	-5.3
Unbiased Group					
Left_Precuneus/PCC	13644	-2	-24	55	-6.9

Right_Cuneus	4554	5	-67	20	-5.4
Right_Insula	2054	44	13	-5	4.7
Right_Inferior_Parietal_Lobule	915	56	-39	39	5
Left_Middle_Frontal_Gyrus	622	-26	29	40	-4.7
Left_Insula	584	-39	12	-9	4.8
Right_Cerebellum	582	33	-37	-30	-4.7
Left_Cerebellum	440	-32	-38	-26	-4.7
Left_Ventromedial Prefrontal	408	1	53	-16	-4.4
Negative Bias Group					
Right_Insula	9402	47	1	10	4.1
Left_Precentral_Gyrus	6015	-28	-27	56	-5.5
Right_Precentral_Gyrus	2462	47	-15	47	-4.8
Left_Insula	2025	-42	8	-6	5.8
Left_Precuneus	1057	-1	-56	16	5
Left_Middle_Occipital_Gyrus	845	-40	-75	27	-4.6
Left_Inferior_Parietal_Lobe	716	-59	-40	37	5
Left_Ventromedial Prefrontal	568	-5	61	-9	-4.9
Right_Middle_Occipital_Gyrus	552	42	-77	30	-4.5
Left_Superior_Frontal_Gyrus	552	-22	37	39	-4.8
Right_Anterior_Cingulate_Cortex	431	4	25	40	4.6
Left_Cerebellum	406	-28	-36	-29	-4.6

References

[1] Craig AD. How do you feel? Interoception: the sense of the physiological condition of the body. NatRevNeurosci 2002;3(8):655-666.

[2] Craig AD. How do you feel?: an interoceptive moment with your neurobiological self: Princeton University Press, 2015.

[3] Faillenot I, Heckemann RA, Frot M, Hammers A. Macroanatomy and 3D probabilistic atlas of the human insula. Neuroimage 2017;150:88-98.

[4] Fields HL. How expectations influence pain. Pain 2018;159 Suppl 1:S3-S10.

[5] Hammers A, Allom R, Koepp MJ, Free SL, Myers R, Lemieux L, Mitchell TN, Brooks DJ, Duncan JS. Three-dimensional maximum probability atlas of the human brain, with particular reference to the temporal lobe. Hum Brain Mapp 2003;19(4):224-247.

[6] Misaki M, Kim Y, Bandettini PA, Kriegeskorte N. Comparison of multivariate classifiers and response normalizations for pattern-information fMRI. Neuroimage 2010;53(1):103-118.

[7] Strigo IA, Matthews SC, Simmons AN. Decreased frontal regulation during pain anticipation in unmedicated subjects with major depressive disorder. Translational Psychiatry 2013;3(3):e239.